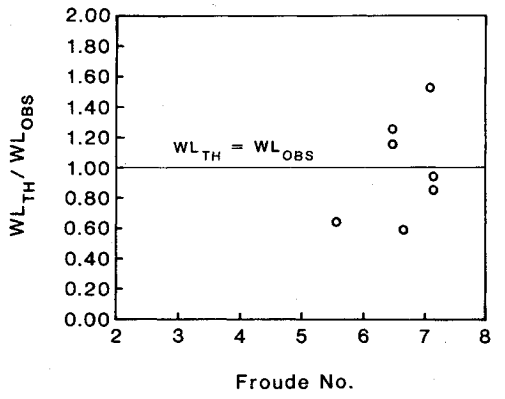

Fig. 6 Comparison of theoretical and observed wake lengths.

proaches pool film boiling, in which vapor is removed from the wake by a Taylor instability mode. The potential flow theory does not account for this behavior; thus, only data at $Fr > 5$ were retained in Fig. 6.

In our opinion, the scatter in the data is largely caused by the competing effects of buoyancy and inertia. Systematic uncertainty due to pressure sensor and recording errors was estimated at $\pm 5\%$, much less than the scatter inherent in the data. Limitations on liquid velocity would not allow data to be obtained in the $Fr \geq 10$ range.

The theory is not very accurate near the end of the wake because of the artificiality of the wake closure model. Taking this into account, the WL predictions shown in Fig. 6 exhibit reasonable conformity with experiment. However, the data are scattered; they cluster about the line of perfect agreement with a variance of 10%. Data for $Fr \geq 10$ are needed for more conclusive evidence of the applicability of the model, but could not be obtained with our apparatus.

WT at the point of separation could not be measured because the heater mounts obscured the end view of the heater. However, an "effective" WT_{obs} was calculated based on the Δp required to predict WL_{obs}. A comparison of this value to WT_{th} calculated from the measured Δp showed that WT is less sensitive to p_{wk} than is WL and is predicted by the theory quite well. This is so because the theory is more accurate near the trailing edge of the cylinder.

Conclusions

The conclusions that have been reached in this study are:

1) Film boiling wakes are not substantially different than cavitation wakes. However, for prediction, the proper θ_s and p_{wk} must be known.

2 The re-entrant jet theory predicts film boiling wake behavior reasonably well.

3) Wake shapes computed from the theory agree qualitatively with observations of subcooled flow film boiling wakes. The theory predicts that WL and WT are reduced as subcooling in the liquid is increased at a given liquid velocity, which agrees with prior observations.

Acknowledgments

Both authors appreciate the support of the National Science Foundation under Grants MEA 8008036 and MEA 8411894 during this research program.

References

[1]Bromley, L.A., "Heat Transfer in Stable Film Boiling," *Chemical Engineering Progress,* Vol. 46, 1950, pp. 221-227.

[2]Bromley, L.A., LeRoy, N.R., and Robbers, J.A., "Heat Transfer in Forced Convection Film Boiling," *Industrial and Engineering Chemistry,* Vol. 45, 1953, pp. 2639-2645.

[3]Epstein, M. and Hauser, G., "Subcooled Forced Convection Film Boiling in the Forward Stagnation Region of a Sphere or Cylinder," *International Journal of Heat and Mass Transfer,* Vol. 23, 1980, pp. 179-189.

[4]Witte, L.C. and Orozco, J., "The Effect of Vapor Velocity Profile Shape on Flow Film Boiling from Submerged Bodies," *Journal of Heat Transfer,* Vol. 106, No. 1, Feb. 1984, pp. 191-197.

[5]Sideman, S., "The Equivalence of the Penetration Theory and Potential Flow Theories," *Industrial and Engineering Chemistry,* Vol. 58, No. 2, 1966, pp. 54-68.

[6]Gurevich, M.I., *Theory of Jets in Ideal Fluids* (translated from Russian), Academic Press, New York, 1965, pp. 181-242.

[7]Chaplygin, S.A., "Gas Jets," *Scientific Memoirs,* Moscow University, Moscow, 1962 (translated as NACA TM 1063, 1944).

[8]Kaul, R., "Hydrodynamics of Wakes Caused by Film Boiling," MS Thesis, Dept. of Mechanical Engineering, University, of Houston, TX, May 1985 (also AIAA Paper 85-1043, June 1985).

[9]Orozco, J., "Flow Film Boiling from Submerged Bodies," Ph.D. Dissertation, Dept. of Mechanical Engineering, University of Houston, TX, Dec. 1984.

[10]Lienhard, J.H., Eichhorn, R., Hasan, M.M., and Hasan, M.Z., "Boiling Burnout During Crossflow over Cylinders, Beyond the Influence of Gravity, *Journal of Heat Transfer,* Vol. 103, 1981, pp. 478-484.

Determination of the Cross-Sectional Temperature Distribution and Boiling Limitation of a Heat Pipe

G.P. Peterson*
Texas A&M University, College Station, Texas

PRESENTLY, the primary means for rejecting heat from orbiting spacecraft is through a space radiator system composed of a series of single-phase fluid loops. Because this system uses a mechanically pumped coolant circuit, it is one whose long-mission reliability is low due to failure resulting from penetration by a single meteroid. The reliability of the system can be increased, but this results in a large increase in total weight. Hence, there is need for the development of a long-life heat rejection system suitable for long-term, high-power missions.

One solution to this problem is to develop a large modular radiator system that can be assembled during orbit from a number of standard components. This "space-constructible" radiator system would fulfill the needs and demands of large long-lived heat rejection systems by allowing the radiators to be built up for any desired heat load capacity. The planned system consists of individual heat pipes with radiator fins attached. These heat pipes would form the radiator and would be "plugged in" to contact heat exchangers designed to carry heat from the habitation module to the radiator through a centralized fluid loop.

Received Oct. 16, 1985; revision received July 3, 1986.

*Assistant Professor of Mechanical Engineering. Member AIAA.

A key component of this concept is a high-capacity heat pipe such as the one developed by Grumman Aerospace Corporation.[1] This improved high-performance heat pipe is shown in Fig. 1 and has two large axial channels, one for vapor flow and another for liquid flow. These two channels are separated by a small monogroove slot that, due to the small characteristic radius, results in the liquid being pumped from the liquid channel to the circumferential grooves in the vapor channel, where it is evaporated. The separation of the liquid and vapor flows reduces the viscous shear force between the liquid and vapor and, hence, increases the overall transport capacity.

This heat pipe is currently being considered for large orbiting space platforms; previous analytical investigations[2] have been conducted to determine the operational characteristics and transport limitations. The results from these investigations have been correlated with the results of a series of experimental investigations,[1,3] and have proved to be reasonably accurate up to that point where the input heat flux limitation is reached and nucleate boiling begins.

In this particular heat pipe, boiling spreads very rapidly since a bubble in any one of the individual circumferential grooves effectively seals off that groove and results in a localized hot spot, causing boiling to occur in the adjacent circumferential grooves. The result is a very rapid reduction in the heat pipe performance. In addition to boiling in the circumferential grooves, previous experimental data seemed to indicate that bubbles forming in the monogroove slot were inhibiting the flow of liquid and contributing to premature limitations on the transport capacity.

Analysis

A two-step approach was used to investigate this boiling phenomenon. First, a two-dimensional, steady-state, finite-element analysis was performed[4] to determine the cross-sectional temperature distribution and the extent to which boiling was present in the circumferential grooves and the monogroove slot. Second, experimental tests were conducted to provide data for verifying the model.

In the analysis, the monogroove heat pipe cross section was divided into 38 rectangular elements with 188 individual nodal points. The heat pipe was assumed to be operating under steady-state conditions with three types of boundary conditions: heat flux addition across the top surface of the fin, convection on the inside of the liquid channel, vapor channel, and monogroove slot, and insulation on the remaining surfaces.

The finite-element governing equations for the heat pipe can be written as

$$(\boldsymbol{K}^k + \boldsymbol{K}^c)^{t+\Delta t}\theta = {}^{t+\Delta t}\boldsymbol{Q} + {}^{t+\Delta t}\boldsymbol{Q}^e \tag{1}$$

where $\boldsymbol{K}^k$ is the conductivity matrix, $\boldsymbol{K}^e$ the convection matrix, $\boldsymbol{Q}^e$ the nodal point heat flux input vector, and θ the temperature vector. The convection matrix $\boldsymbol{K}^c$ and the convection boundary conditions $\boldsymbol{Q}$ are treated as extra conductivity and heat flux loading terms and are added to $\boldsymbol{K}^k$ and $\boldsymbol{Q}$, respectively. These two values can be found for an element m as

$$\boldsymbol{K}^c = \sum_m \int_{S_c(m)} h^{(m)} \boldsymbol{H}^{S(m)T} \boldsymbol{H}^{S(m)} \mathrm{d}S^{(m)} \tag{2}$$

$${}^{t+\Delta t}\boldsymbol{Q}^e = \sum_m \int_{S_c(m)} h^{(m)} \boldsymbol{H}^{S(m)T} \boldsymbol{H}^{S(m)t+\Delta t}\theta_e \mathrm{d}S^{(m)} \tag{3}$$

where $\boldsymbol{H}^s$ is the surface temperature shape function, h the convection coefficient, θ^e the environmental temperature, and S_c the convection boundaries.[4]

Using this analysis technique, the cross-sectional temperature distribution was calculated. Once this had been accomplished, lines of constant temperature were established for various adverse tilts and input power levels. These lines of constant temperature were then used to determine the point at which boiling was most likely to occur, as well as the location and extent of dryout.

Initially, a three-dimensional model was formulated. However, during the development of the model, it became apparent that a two-dimensional heat-transfer model with linear, steady-state conditions would be adequate, assuming that the cross-sectional shape of the heat pipe was constant and that the temperature and pressure variations along the longitudinal axis of the evaporator section of the heat pipe were small over the anticipated operating range.

It is apparent from the geometry that the assumption of constant cross-sectional shape is valid and the temperature variation along the evaporator section of the heat pipe can be found by neglecting the frictional effects and applying the energy conservation principle. This yields

$$\frac{T_v(0)}{T_v} = 1 + \frac{V_v^2}{2C_p T_v} \tag{4}$$

or

$$T_v(0) = T_v + \frac{V_v^2}{C_p} \tag{5}$$

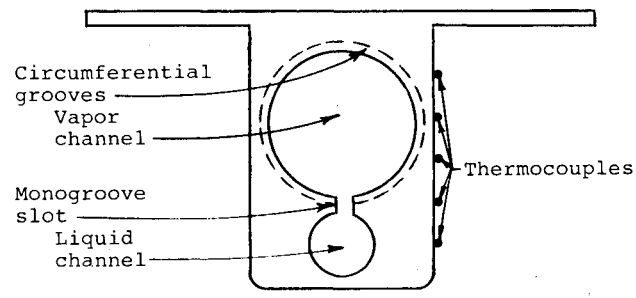

Fig. 1 Monogroove heat pipe and thermocouple locations.

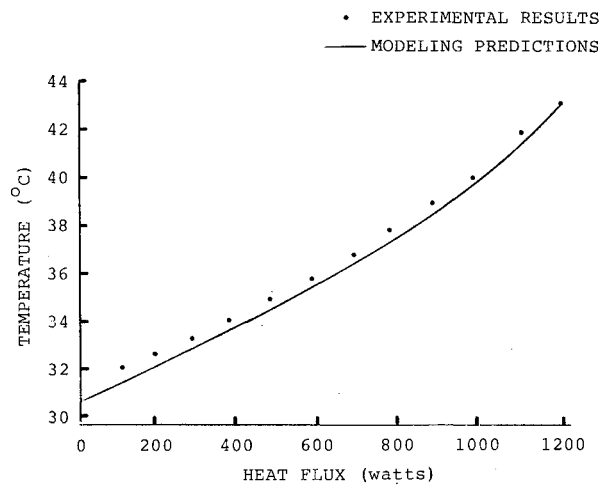

Fig. 2 Comparison of predicted and measured temperature, top thermocouple.

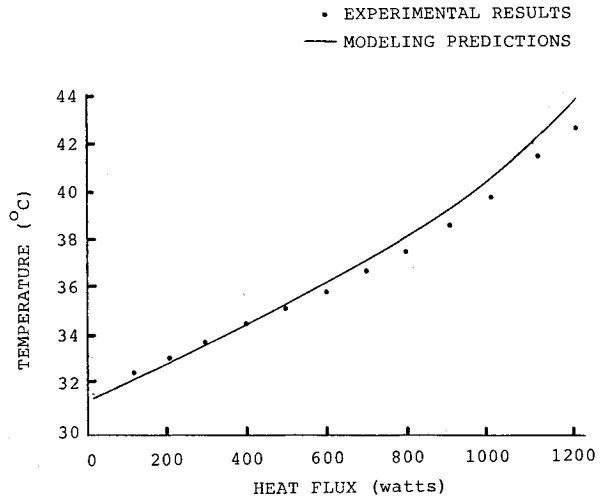

Fig. 3 Comparison of predicted and measured temperature, middle thermocouple.

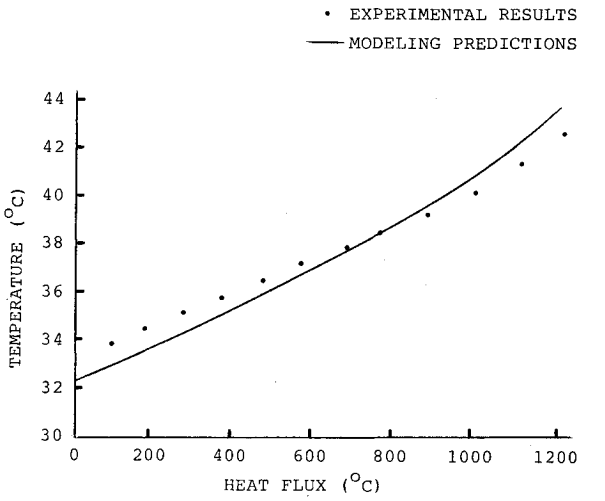

Fig. 4 Comparison of predicted and measured temperature, bottom thermocouple.

where $T_v(0)$ is the vapor temperature at that point where the vapor velocity is zero (i.e., one end of the evaporator), T_v (max) the vapor temperature at that point where the vapor velocity is a maximum (i.e., the other end of the evaporator), and C_p the specific heat at constant pressure. From Eq. (5), the total temperature drop in the evaporator section ΔT_e is

$$\Delta T_e = T_v(\max) - T_v(0) = \frac{V_v^2}{2C_p} \tag{6}$$

In the operating range of this particular heat pipe, the vapor velocity is very small, approximately 1 m/s; however, C_p has a value three orders of magnitude greater, which results in a temperature gradient that is quite small. In order for the temperature gradient to be significant, the vapor velocity needs to be an order of magnitude greater, in which case the heat pipe would be approaching the sonic limitation.

Test Procedure

In order to verify the accuracy of the modeling technique, an experimental investigation was conducted using a 3.05 m section of the heat pipe. The fin on the test section was 5.7 cm wide, the vapor channel and liquid channel diameters were 1.524 and 1.016 cm, respectively, and the monogroove slot was 0.254 mm wide and 1.24 mm deep. Five thermocouples were located approximately 10 cm from the condenser end of the evaporator, equally spaced along the outer sidewall of the heat pipe, as shown in Fig. 1. Heat was applied to the evaporator section using an electric resistance heater and a simple electrical measurement was used to determine the input power. Heat removal was accomplished using a single-phase liquid coolant circuit.

The tests were conducted using a computerized data acquisition and logging system to gather and compile the various measurements. The data acquisition system consisted of a Hewlett-Packard 87 computer as the system controller, a Fluke 2190A digital thermometer (acting with a Fluke 2300A 20 channel scanner and a Fluke 1120A IEEE-488 translator) as the thermocouple interface, two Hewlett-Packard 3438A digital multimeters to measure the heater voltage and current, and a third 3438A to measure the flowmeter signal voltage from an orifice plate flowmeter in the coolant circuit. Once the instrumentation had been installed and tested, the heat pipe and coolant system were wrapped in fiberglass insulation to minimize heat loss to the surroundings.

The test procedure used was as follows. The input power was increased in 100 W increments, from zero to the point where a rapid rise in the temperature of the thermocouples located on the top fin of the evaporator was observed. It was through this rapid temperature rise that the onset of dryout was detected. This procedure was followed at adverse tilts, which varied in 2.5 mm increments from 0 to 1.5 cm, and resulted in a total of 222 instrumented performance tests. At each test point, the system was allowed to reach thermal equilibrium, at which time a series of three data records were taken at 10 min intervals.

Results and Conclusions

Upon completion of the experimental tests, the temperatures recorded by each of the thermocouples on the outer surface of the heat pipe were compared with the modeling predictions. Figures 2–4 illustrate the relationship between the predicted cross-sectional temperature distribution as determined from the computer model and the temperature measured during the experimental tests for the top, middle, and lower thermocouples. Additional correlations were made for the others, but are not presented here. As illustrated, a slight decrease in the accuracy of the modeling predictions occurs as the distance from the upper fin increased and there appears to be a slight shift to the right in the point at which the modeling predictions and the experimental results intersect. The overall accuracy, however, was quite good and was within 1.7°C or 2.8%.

Once it had been demonstrated that the computer model accurately predicted the cross-sectional temperature distribution, additional analyses were conducted and the associated thermal maps were developed for various power levels to determine if boiling was occurring in the monogroove slot. These analyses indicated that bubble formation in the monogroove slot would not occur until approximately 75% of the circumferential groove area had reached dryout, contradicting the original assumption that boiling in the monogroove slot was prematurely limiting the heat pipe. In addition to determining that monogroove boiling was not a problem, the computer model was capable of accurately predicting the location and magnitude of the circumferential dryout condition as a function of the input heat flux.

In summary, a computer model has been developed and verified that is capable of determining the cross-sectional

temperature distribution within the heat pipe. This model can provide information that can be used to determine the susceptibility of the monogroove heat pipe to boiling, along with the location and magnitude of that boiling.

Acknowledgment

Funding for this work was provided under NASA Contract NAS 84-496.

References

[1]Alario, J., Haslet, R., and Kosson, R., "The Monogroove High Performance Heat Pipe," AIAA Paper 81-1156, June 1981.

[2]Peterson, G.P., "Computer Modeling and Simulation of Dual Passage Heat Pipes during Steady State Operation," NASA Final Rept. NTG 44-005-115, July 1981.

[3]Peterson, G.P., "Heat Pipe Modeling and Simulation," AIAA Paper 85-0152, Jan. 1985.

[4]Bathe, K.J., *Finite Element Procedures in Engineering Analysis*, 1st ed., Prentice-Hall, Englewood Cliffs, NJ, 1982.